Title

CUB Domain-Containing Protein 1 (CDCP1) Is a Target for Radioligand Therapy in Castration-Resistant Prostate Cancer, including PSMA Null Disease.

Journal

Clinical Cancer Research, 28(14)

ISSN

1078-0432

Authors

Zhao, Ning
Chopra, Shalini
Trepka, Kai
et al.

Publication Date

2022-07-15

DOI

10.1158/1078-0432.ccr-21-3858

Peer reviewed

Published in final edited form as:

Clin Cancer Res. 2022 July 15; 28(14): 3066–3075. doi:10.1158/1078-0432.CCR-21-3858.

CUB domain containing protein 1 (CDCP1) is a target for radioligand therapy in castration resistant prostate cancer including PSMA null disease

Ning Zhao[1], **Shalini Chopra**[1], **Kai Trepka**[2], **Yung-hua Wang**[1], **Sasank Sakhamuri**[1], **Nima Hooshdaran**[1], **Hyunjung Kim**[1], **Jie Zhuo**[3], **Shion A. Lim**[3], **Kevin K. Leung**[3], **Emily A. Egusa**[4,6], **Jun Zhu**[4,6], **Li Zhang**[2], **Adam Foye**[4], **Renuka Sriram**[1], **Emily Chan**[5], **Youngho Seo**[1], **Felix Y. Feng**[4,6], **Eric J. Small**[2,6], **Jonathan Chou**[2,6], **James A. Wells**[3,6], **Rahul Aggarwal**[2,6], **Michael J. Evans**[1,3,6]

[1]Department of Radiology and Biomedical Imaging, University of California, San Francisco, San Francisco, CA 94158.

[2]Department of Medicine, University of California, San Francisco, San Francisco, CA 94158.

[3]Department of Pharmaceutical Chemistry, University of California, San Francisco, San Francisco, CA 94158.

[4]Department of Radiation Oncology, University of California, San Francisco, San Francisco, CA 94158.

[5]Department of Pathology, University of California, San Francisco, San Francisco, CA 94158.

[6]Helen Diller Family Comprehensive Cancer Center, University of California, San Francisco, San Francisco, CA 94158.

Abstract

Purpose: With the improvement in overall survival with 177Lu-PSMA 617, radioligand therapy (RLT) is now a viable option for patients with metastatic castration resistant prostate cancer (mCRPC). However, responses are variable, in part due to low PSMA expression in 30% of patients. Herein, we evaluated if the cell surface protein CUB domain containing protein 1 (CDCP1) can be exploited to treat mCRPC with RLT, including in PSMA low subsets.

Experimental Design: CDCP1 levels were evaluated using RNA-seq from 119 mCRPC biopsies. CDCP1 levels were assessed in 17 post enzalutamide or abiraterone treated mCRPC biopsies, 12 patient derived xenografts (PDX), and prostate cancer cell lines. 4A06, a recombinant human antibody that targets the CDCP1 ectodomain, was labeled with Zr-89 or Lu-177 and tested in tumor bearing mice.

Results: CDCP1 expression was observed in 90% of mCRPC biopsies, including small cell neuroendocrine (SCNC) and adenocarcinomas with low FOLH1 (PSMA) levels. Fifteen of 17 evaluable mCRPC biopsies (85%) demonstrated membranous CDCP1 expression, and 4 of 17

Corresponding authors: Name: Michael J. Evans, PhD, Address: 600 16th Street, N572C, San Francisco, CA 94158, Telephone: 415-514-1292, michael.evans@ucsf.edu, Name: Rahul Aggarwal, MD, Address: 550 16th Street, 6th Floor, Telephone: 415-353-7171, rahul.aggarwal@ucsf.edu.

(23%) had higher CDCP1 H-scores compared to PSMA. CDCP1 was expressed in ten of twelve PDX samples. Bmax values of ~22,000, ~6,200, and ~2,800 fmol/mg were calculated for PC3, DU145, and C4-2B human prostate cancer cells respectively. 89Zr-4A06 PET detected six human prostate cancer xenografts, including PSMA low tumors. 177Lu-4A06 significantly suppressed growth of DU145 and C4-2B xenografts.

Conclusions: The data provide the first evidence supporting CDCP1-directed RLT to treat mCRPC. Expanded studies are warranted to determine if CDCP1 is a viable drug target for mCPRC patients.

Statement of Translational Relevance:

New targets for radioligand therapy (RLT) are needed given the primary and acquired resistance observed with current strategies including PSMA-directed radioligands. This study advances CDCP1 as a novel target for metastatic castration resistant prostate cancer, in both adenocarcinoma and neuroendocrine subtypes. Combined with low expression in normal human tissues, these data provide a compelling scientific rationale for translating CDCP1-directed RLT into the clinic, either alone or in combination with other therapies, for treating advanced prostate cancer patients.

Keywords

Theranostics; endoradiotherapy; molecular imaging; antibody

Introduction

Radioligand therapy (RLT) as a treatment modality is currently undergoing a renaissance, fueled in part by advances in “-omic” technologies to better identify tumor specific protein targets, a stronger understanding of the features of ligand design required to minimize dose limiting toxicity, and a larger repertoire and supply of therapeutically beneficial radioisotopes, including α particle emitters (e.g. Ac-225, Ra-223) (1). Moreover, the recent FDA approvals of Lutathera for neuroendocrine tumors, Azedra for pediatric malignancies, and the breakthrough designation bestowed on ^{177}Lu-PSMA 11 for the treatment of metastatic castration resistant prostate cancer (mCRPC) strongly suggest that RLT may be scalable approach for the treatment of many deadly cancers(2–6). That said, tumor responses to the abovementioned RLTs can be limited in duration, in part due to dose limiting toxicity, intrinsic or acquired tumor resistance, and the heterogeneity of protein target expression on tumor cells (7). Therefore, there is an urgent unmet need to identify strategies to overcome these limitations.

While the clinical data with ^{177}Lu-PSMA 11 and bone-seeking radionuclides (i.e. Ra-223, Sm-153) show that mCRPC is a radiosensitive tumor type, there are intrinsic limitations for these RLTs. For example, bone-seeking radionuclides cannot treat soft tissue tumors. Moreover, the radiometals accumulate in the bony tissue adjacent to the tumor cell, rather than within the tumor cell, and the subsequent radiographic responses in bony metastases are transient. PSMA-directed RLT is not suitable for treating low-PSMA expressing mCRPC including treatment-emergent small cell neuroendocrine cancer (t-SCNC), a subset of

mCRPC observed in up to 15–20% of cases (8). PSMA is also not selectively expressed by mCRPC, and on-target, off-tissue effects of PSMA-directed RLT (e.g. xerostomia) are well documented, limiting treatment duration and overall quality of life. Collectively, these observations provide a strong scientific rationale for exploring new RLTs to improve treatment outcomes in mCRPC.

Recent discoveries about its expression in prostate cancer and proof of concept studies demonstrating it can be targeted for RLT in other cancer types (e.g. pancreatic cancer) led us to hypothesize that the single pass transmembrane protein CUB domain containing protein 1 (CDCP1) could be potential target for RLT that overcomes some of the abovementioned limitations. CDCP1 overexpression commonly occurs in human prostate cancer cell lines and in a recent study, was shown to be overexpressed in ~50% of metastatic biopsies and ~30% of primary tumors (9–11). CDCP1 overexpression was significantly associated with PTEN loss and a more aggressive phenotype. These data coincide with a growing movement to target CDCP1 for cancer treatment using various antibody-based therapeutic modalities (12, 13). We and others have shown that various antibodies (e.g. IgG12, IgG58, 4A06, 10D7) targeting the ectodomain of CDCP1 can be functionalized with diverse payloads (cytotoxins, Lu-177, Ac-225) to confer antitumor effects with negligible host toxicity due to on target, off tissue binding or off target effects (10, 12, 14–16). Building on this momentum, we endeavored herein to test if CDCP1 can be targeted for RLT in mCRPC, particularly for the subset of the disease that would be expected to be refractory to bone seeking radionuclides and/or PSMA-directed RLT.

Material and Methods

General Methods:

All data presented in this study are available upon request. All materials and chemicals were purchased from commercial vendors and used without further processing/purification. DU145, 22RV1, C4-2B, and PC3 cell lines were obtained from American Type Tissue Collection (ATCC) and cultured according to manufacturer's recommendations. Cellular identity was authenticated by visually inspecting morphology and probing for signature expression markers on immunoblot. Mycoplasma contamination was tested within the first two passages after thawing cryostocks with the MycoAlert kit (Lonza). All cells were studied between passages 5 to 25. The monoclonal antibody 4A06 was expressed and purified in the IgG1 format as previously described (13). p-SCN-Bn-Deferoxamine (B-705) and p-SCN-Bn-DOTA (B-205) were purchased from Macrocyclics (Plano, TX). ^{89}Zr-oxalate was obtained from 3D Imaging, LLC (Maumelle, AR). $^{177}LuCl_3$ was obtained from Oak Ridge National Laboratory. Iodine-125 was obtained from Perkin Elmer. ^{68}Ga-PSMA 11 was prepared by the radiopharmacy at UCSF according to previously reported protocol (17). LTL xenograft samples were acquired form Living Tumor Laboratory (Vancouver, BC) and the LuCaP xenograft series was provided by Dr. Eva Corey at University of Washington.

Analysis of Patient Biopsies:

Written informed consent was obtained prior to collecting patient biopsies. The sample collection and analysis were performed in accordance with the ethical guidelines stipulated

in the Declaration of Helsinki, and the study was review and approved by the Institutional Review Board at UCSF prior to its start. Recently acquired metastatic biopsies from mCRPC patients clinically annotated with survival data was used for analysis (18, 19). Patient samples were obtained using image-guided core needle biopsy of metastatic lesion in the bone or soft tissue. Laser capture microdissection was used to isolate samples enriched for cancer, with cores freshly frozen for RNA sequencing, and separate core formalin-fixed and paraffin embedded for immunohistochemical analysis.

SCNC status was determined via unsupervised hierarchical clustering using a previously validated gene signature and confirmed via evaluation by three experienced pathologists blinded to the clinical and genomic features for determination of consensus pathologic subclassification(19). The following list of genes was used for hierarchical clustering to determine SCNC status: AR, TMPRSS2, GATA2, HOXB13, KLK3, FOXA1, NKX3–1, CHGB, FOXA2, SOX2, SCG2, NKX2–1, REST, SPDEF, NOTCH2, NOTCH2NL, ASCL1, ETV1, ETV4, ETV5, RB1, CDKN2A, E2F1. Linear regression between *CDCP1* and *FOLH1* expression was performed in R (v4.0.2), with the resulting P value and Pearson correlation coefficient reported.

The needle biopsies were fixed in 10% formalin overnight, transferred to 70% ethanol the next day, and then processed for paraffin embedding and sectioning. Sections of formalin-fixed, paraffin embedded (FFPE) tissue were placed into the Ventana Discovery Ultra automated slide stainer. Antigen retrieval was performed using heat-inactivated antigen retrieval buffer (Tris-EDTA) according to the manufacturer instructions (Roche) and then stained with the following primary antibodies: rabbit polyclonal CDCP1 (Cell Signaling Technology, #4115S, 1:50), mouse monoclonal PSMA (Dako Agilent, M3620 clone 3E6, 1:100) or rabbit monoclonal CD3 (Ventana clone 2GV6, #790–4341, 1:100) for 32 minutes at 36°C. Secondary antibodies (Anti-Rabbit HQ, Anti-Mouse alk phos, HQ-HRP, Purple HRP and Yellow AP for dual chromogenic stains, all from Ventana) were incubated for 12 min each, and DAB was used for detection for single stains. Slides were counterstained with hematoxylin per standard protocol. H-scores for CDCP1 and PSMA membrane staining were assigned by two independent pathologists (1+, 2+ and 3+ multiplied by the percentage), and the average of the H-scores was calculated.

Flow Cytometry:

Actively proliferating cells were lifted mechanically from a tissue culture plate and placed in the primary antibody solution diluted in PBS (4A06, 1:1,000). After a 30 min incubation, the cells were washed with PBS multiple times and placed in a fluorophore conjugated secondary antibody solution for 30 minutes on ice (1:500, 109-546-097, Jackson ImmunoResearch). Cells were collected and washed before being placed in PBS and passed through a cell strainer. Samples were taken to a flow machine (FACS CantoII). Data analysis was performed using FlowJo.

Immunoblot:

Tumor samples were added to Pierce RIPA lysis buffer (89900, ThermoFisher Scientific) with Halt protease and phosphatase inhibitors (1861281, ThermoFisher Scientific). The

samples were homogenized using a probe sonicator (Omni TH-01) and then centrifuged for 15 minutes at 15,000 ×g. 4X SDS-loading buffer was added to protein lysates and 15 μg of lysate were resolved on a 4–12% Bis Tris gel (NW04120BOX, Invitrogen). Gels were transferred onto an Immobilon-P membrane (IPVH00010, Millipore). Membranes were blocked in 5% milk in TBST for 90 minutes before being placed in a primary antibody solution. Primary antibodies used were CDCP1 (4115, Cell Signaling, 1:1000), PSMA (12815, Cell Signaling, 1:1000), and B-Actin (A5441, Sigma-Aldrich, 1:5000). Membranes were then washed and incubated with a secondary antibody solution for 30 min at room temperature. Secondary antibodies used were goat anti-rabbit (65-6120, Invitrogen, 1:5000) and goat anti-rat (62-6520, Invitrogen, 1:5000). Proteins were detected using West Pico Chemiluminescent Substrate for 20 seconds (34578, ThermoFisher Scientific) and then exposed to film (30-507, Blue Devil). Each immunoblot was reproduced at least once with freshly harvested protein samples.

Saturation binding assays:

To prepare ^{125}I-4A06, 6.0 μL of ^{125}I in 1M NaOH (~ 340 uCi) was added into a vial containing 100.0 μL of HEPES buffer (0.5 M). This solution was transferred to an iodination tube (Peirce) and 4A06 antibody (300μg) was then added. The tube was incubated for 10 min at room temperature, and ITLC showed 85.0% radiolabeling efficiency (solvent: 20nM citric acid). ^{125}I-4A06 was purified using a G-25 column. The final yield of the purified ^{125}I-4A06 was 68.58% (specific activity =1.13 μCi/μg) and purity was > 99%.

DU145 and PC3 (0.6×10^6 cell/well) were seeded on 12-well plates using DMEM (10% FBS). The cells were washed with PBS for the saturation binding assay. Total binding of ^{125}I-4A06 was determined by adding it to cell suspensions at seven concentrations from 0.025 nM to 10 nM. Non-specific binding was determined by adding 1000x cold 4A06 to ^{125}I-4A06/cell mixtures at 0.025nM, 0.3 nM, and 10 nM. In all cases, cells were incubated with ^{125}I-4A06 at room temperature for 1 hr, washed with PBS, and lysed by adding 1.0 M NaOH. The bound and unbound radioactive fractions were collected and measured on a Hidex Gamma counter (Turku, FI). Bmax was calculated using Prism v8.0.

Animal studies:

All animal studies, including housing and welfare monitoring, were conducted in compliance with Institutional Animal Care and Use Committee at UCSF. Animal imaging studies involving patient derived xenografts (PDX) utilized eight to ten week old intact male NOD SCID gamma (NSG) mice from Charles River Laboratory. PDX lines were obtained from the Living Tumor Lab at the Vancouver Prostate Centre. For tumor imaging or treatment studies with mCRPC xenografts from cell line implants, four to six-week-old intact male athymic nu/nu mice (Charles River) were utilized. Mice were inoculated subcutaneously (~1.5×10^6 cells) in the flank with a slurry of cells in 1:1 mixture (v/v) of media (DMEM) and Matrigel (Corning). Xenografts were generally palpable within 3–4 weeks after injection. Tumor bearing mice received ~300 μCi of ^{89}Zr-406 or ~300 μCi of ^{68}Ga-PSMA 11 for imaging studies. Mice bearing subcutaneous DU145 tumors received ^{177}Lu-4A06 (400 μCi) or vehicle (saline) via tail vein at day 0 and day 5 of the study period, which was approximately 14–21 days post tumor inoculation. Mice bearing subcutaneous

C4-2B tumors received ^{177}Lu-4A06 (300 μCi) or vehicle (saline) via tail vein at day 0 and day 5 of the study period, which was approximately 14–21 days post tumor inoculation. Mice were arranged in treatment arms using a simple randomization approach (20). Animals were weighed at the time of injection, and once weekly until the completion of the study. Tumor volume measurements were calculated with calipers. The study endpoints were death due to tumor volume >2000 mm^3 or ≥ 20% loss in mouse body weight. The researcher performing the tumor volume and body weight measurements was blinded to the treatment arms.

Small animal PET/CT:

4A06 was functionalized with desferrioxamine (DFO) and subsequently radiolabeled with Zr-89 as previously described (14). Tumor-bearing mice received ~200 μCi of ^{89}Zr-4A06 in 100 μL saline solution volume intravenously using a custom mouse tail vein catheter with a 28-gauge needle and a 100–150 mm long polyethylene microtubing. Mice were imaged on a small animal PET/CT scanner (Inveon, Siemens Healthcare, Malvern, PA). Animals were typically scanned for 30 minutes for PET, and the CT acquisition was performed for 10 minutes.

The co-registration between PET and CT images was obtained using the rigid transformation matrix generated prior to the imaging data acquisition since the geometry between PET and CT remained constant for each of PET/CT scans using the combined PET/CT scanner. For microPET/CT data, PET images were reconstructed using the ordered subsets expectation maximization algorithm (OSEM) provided by the scanner manufacturer. The parameters for OSEM were 16 subsets and 4 iterations, and the resulting reconstructed image volume was in a matrix of 128×128×159 with a voxel size of 0.0776 mm × 0.0775 mm × 0.0796 mm. CT images for attenuation correction were reconstructed using a conebeam Feldkamp algorithm provided by the scanner manufacturer. The data were acquired using x-ray tube voltage of 80 kVp and current of 0.5 mA for 120 angular steps over 220 degrees, and 175 ms of exposure at each angular step. The reconstructed CT volume was in a matrix of 512×512×700 with a voxel size of 0.195 mm × 0.195 mm × 0.195 mm. The precalibrated scaling was used to convert the CT images to attenuation maps for correction in PET reconstruction.

For SUV computation, we used freeware software, Amide (amide.sourceforge.net), and used its automated SUV calculation tool by entering decay-corrected injected activity and the animal weight. For each volume of interest, a spherical VOI (2–3 mm diameter) was drawn and SUV was calculated by VOI statistics.

Small animal SPECT/CT: 4A06 was functionalized with DOTA and radiolabeled with Lu-177 as previously described (14).

At 48 hours post injection of the second dose of ^{177}Lu-4A06 (i.e. day 7 overall of the antitumor assessment study), the mice were imaged under anesthesia using a small animal SPECT/CT (VECTor4CT, MILabs, Utrecht, The Netherlands). Animals were typically scanned for 40 minutes for SPECT, and the CT acquisition was performed for 10 minutes. The co-registered CT was used for photon attenuation correction in the SPECT reconstruction. For microSPECT/CT data, SPECT images were reconstructed using

the similarity-regulated OSEM (SROSEM) provided by the scanner manufacturer. The parameters for SROSEM were 128 subsets and 10 iterations in a base voxel size of 1.2 mm. After reconstruction, a Gaussian postfilter with 1.5 mm full-width at half maximum was applied to suppress image noises. SPECT data were acquired using a multipinhole collimator (HE-GP-RM) with an aperture diameter of 3.6 mm that was designed for general purpose to scan both mice and rats with the axial field of view (FOV) of 18 mm and transverse FOV of 28 mm. Multiple bed positions during the data acquisition were used, controlled by the scanner to cover the whole mouse volume. Both photopeaks (171 keV and 245 keV) for Lu-177 with +/−10% energy window was used from the list mode data, and triple window based scatter correction was applied. After the SPECT reconstruction, the SPECT images were registered to the CT images, and attenuation correction using CT-based attenuation map was applied. CT data were acquired using x-ray tube voltage of 55 kVp and current of 0.19 mA for 480 angular steps over 360 degrees, and 75 ms of exposure at each angular step. CT images were reconstructed using the manufacturer provided conebeam Feldkamp algorithm.

Biodistribution studies:

At a dedicated time after radiotracer injection, animals were euthanized by cervical dislocation. Blood was harvested via cardiac puncture. Tissues were removed, weighed and counted on a Hidex automatic gamma counter (Turku, Finland). The activity of the injected radiotracer was calculated and used to determine the total number of counts per minute by comparison with a standard of known activity. The data were background- and decay-corrected and expressed as the percentage of the injected dose/weight of the biospecimen in grams (%ID/g).

Digital autoradiography:

Post mortem, tumors were harvested, transferred to sample boats, and immersed in Tissue–Plus OCT compound (Scigen, Gardena, CA). The tissues were snap frozen at −80° C. The tumor tissue was sectioned into 20 μm slices using a microtome (Leica, Buffalo Grove, IL) and mounted on glass microscope slides. The slides were loaded onto an autoradiography cassette and exposed with a GE phosphor storage screen for 24–72 hours at −20° C. The film was developed and read on a Typhoon 9400 phosphorimager (Marlborough, MA). Images of whole sections were acquired on a VERSA automated slide scanner (Leica Biosystems, Wetzlar, Germany), equipped with an Andor Zyla 5.5 sCMOS camera (Andor Technologies, Belfast, UK). ImageScope software (Aperio Technologies, Vista, CA) is used for creating individual images. Photoshop CS6 software (Adobe Systems, McLean, VA) were used for montage and processing.

Statistical analysis:

Binary comparisons between two treatment arms were made with an unpaired, two-tailed Student’s t-test. Differences at the 95% confidence level ($P < 0.05$) were considered to be statistically significant. Differences at the 95% confidence level were considered statistically significant. Unless otherwise stated, all data were expressed as mean ± standard deviation.

Overall survival was measured from the date of metastatic biopsy in the mCRPC patients. Kaplan-Meier product limit method and log-rank test were used to investigate the relationship between *CDCP1* expression (transcripts per million, TPM) and overall survival, or *CDCP1* expression, *PTEN* mutation status and overall survival. The patient cohort was dichotomized above and below median *CDCP1* expression as well as broken into quartiles of *CDCP1* expression for survival analyses.

Data Availability:

All data are available upon request to the corresponding authors of the study.

Results

CDCP1 is expressed in mCRPC, including SCNC and adenocarcinoma with low levels of PSMA:

We probed our recently published RNA-seq data set of mCRPC biopsies to assess *CDCP1* expression (19). Unlike a previously reported expression analyses by Alimonti et al. (9), the majority of the mCRPC biopsies from this data set were obtained post-abiraterone and/or enzalutamide from bone and soft tissue lesions, reflecting current treatment patterns. *CDCP1* was expressed in 90% of mCRPC biopsies (107 of 119 samples, see Figure 1A). Since Alimonti et al. showed that CDCP1 mRNA and protein levels are upregulated in PTEN null prostate cancer, we tested for a correlation between *CDCP1* and *PTEN*. A Pearson analysis revealed that *CDCP1* levels were modestly, but significantly, inversely correlated (Supplemental Figure 1). We also compared *CDCP1* mRNA levels between patients with wild type PTEN and patients with any type of PTEN mutation (i.e. deletion, inversion, break-end). We found that *CDCP1* is slightly upregulated in PTEN-mutant patients, though the effect is not statistically significant (Table 1).

To understand if CDCP1 is expressed in tumors with low or undetectable PSMA, we next evaluated the distribution of *CDCP1* versus *FOLH1* (PSMA) expressing tumors. A Pearson analysis comparing the *CDCP1* and *FOLH1* expression per tumor showed that there was no significant correlation between the gene expression levels among the patients in the cohort (Figure 1B). Of the 119 tumors, 14 (12%) were predicted to have low or absent *FOLH1* expression and positive *CDCP1* expression. In addition, 93 of 119 (78%) were predicted to be mutually positive, 3 of 119 (3%) were mutually negative, and 9 of 119 (8%) were predicted to be *FOLH1* positive but *CDCP1* negative.

We further evaluated the protein expression of CDCP1 in mCRPC biopsies. Two blinded pathologists reviewed the biopsies for CDCP1 and PSMA staining, and a mean H score was reported. Of 17 evaluable biopsies, 15 (85%) were positive for cell surface expression of CDCP1, with H-score range of 15 – 285 (Figure 1C). Four samples (23%) had a higher mean H-score for CDCP1 compared to PSMA, including one example (biopsy #10) that overexpressed CDCP1 (H-score 285) but did express PSMA. Of note, one sample (biopsy #15) was negative on staining for both CDCP1 and PSMA. Representative stains are shown in Figure 1D.

CDCP1 overexpression was previously shown to be associated with poorer overall survival in mCRPC; therefore, we assessed this relationship in our cohort. In contrast to the former study, we found no significant association between *CDCP1* expression and overall survival in dichotomized cohorts above and below median expression (log-rank p value = 0.2; Supplemental Figure 2A) or by breaking into quartiles of *CDCP1* expression (log-rank p-value = 0.1; Supplemental Figure 2B). We also found no differences in survival when subdividing the patient cohort into subgroups based upon *CDCP1* expression (above vs. below median) and *PTEN* mutation status (wild type vs. mutation), (log-rank p-value = 0.5; Supplemental Figure 2C).

Since CDCP1 protein was already found to be expressed at high levels in the whole cell lysates of several human prostate cancer cell lines (11), we evaluated expression in human PDX whole cell lysates (Supplemental Table 1). Full length and/or cleaved CDCP1 was expressed in four of five adenocarcinoma PDX models that we tested from the LuCaP and Living Tumor Laboratory series (Figure 2A). The highest levels were observed in LuCaP70 CR and LTL-484, an AR-expressing adenocarcinoma sample with negligible PSMA expression. CDCP1 expression was detected in six of seven SCNC PDXs, with the highest expression observed in LTL-545 and LTL-370 (Figure 2B). In line with some recent reports suggesting that proteolytically cleaved CDCP1 may contribute to early tumor development and metastatic potential (21–23), this proteolytic isoform of CDCP1 was detected in 4 of the 12 PDX samples (LuCaP70 CR, LuCaP 77 CR, LTL484, LTL545).

We next confirmed surface CDCP1 expression in prostate cancer cells using flow cytometry (Figure 2C). The relative cell surface levels in six human prostate cancer cell lines (PC3 > DU145 > C4-2B > LNCaP-AR > CWR22Pc > 22Rv1) approximated previously reported relative levels of total expression on immunoblot (11). To quantify CDCP1 receptor number per cell, we performed saturation binding assays using 4A06, a monoclonal recombinant human antibody that recognizes a region of the CDCP1 ectodomain present in both full length and cleaved CDCP1 (13). We calculated PC3 cells to have a B_{max} of 22,377 fmol/mg (~1.2×10^6 receptors per cell), DU145 to have a B_{max} of 6819 fmol/mg (~3.7×10^5 receptors per cell) and C4-2B to have a B_{max} of 2897 fmol/mg (~1.5×10^5 receptors per cell, see Figure 2D). These values equal or exceed receptor densities reported for PSMA in human prostate cancer cell lines like LNCaP and MDA PCa 2b (~1×10^5 receptors/cell) (24).

Tumor autonomous expression of CDCP1 in mCRPC is detectable with ^{89}Zr-4A06 PET/CT:

We next assessed CDCP1 expression in vivo using ^{89}Zr-labeled 4A06, an IgG1 monoclonal antibody that we previously developed that recognizes an epitope in the ectodomain found on both full-length and cleaved forms of CDCP1 (13). 4A06 was functionalized with desferrioxamine B and radiolabeled to high yield with Zr-89 using our previously reported method (14). We then evaluated tumor uptake over time in intact male nu/nu mice bearing subcutaneous C4-2B tumors (n = 4). Tumoral uptake of ^{89}Zr-4A06 was significantly higher than blood levels at 24 hours post injection (Figures 3A and 3B). Although tumoral uptake did not significantly change between 24 and 48 hours post injection, region of interest analysis suggested the tumor to blood ratio improved from 24 to 48 hours post injection.

As our previous experience with ^{89}Zr-4A06 suggested tumoral uptake typically peaks from 48–72 hours post injection, we next profiled CDCP1 expression at 48 hours post injection in intact male nu/nu or NSG mice bearing DU145, 22Rv1, LTL-545, LTL-331, or LTL-484 tumor xenografts (n = 4/tumor). These tumors represent AR-positive adenocarcinoma (22Rv1, LTL-331, LTL-484) and AR-null disease (DU145, LTL-545). ^{89}Zr-4A06 PET showed clear evidence of radiotracer accumulation in tumors above background levels in blood or skeletal muscle (Figure 3C). Post mortem biodistribution measurements at 48 hours post injection showed that DU145 had the highest radiotracer uptake at 12.9 ± 1.9% ID/g (Figure 3D and Supplemental Figure 3). The tumor to muscle ratios were at least 7:1 and DU145 had the highest ratio at ~25:1 (Supplemental Figure 4). The tumor to blood ratios were at least 2:1 and the LTL-331 cohort had the highest mean ratio of ~70:1 (Supplemental Figure 4). The blood values in the NSG cohorts were lower than those observed in the nu/nu cohorts, which is likely due to high splenic uptake of the IgG as has been previously noted (25). Digital autoradiography was performed to assess radiotracer distribution within a tumor representing high (DU145) and comparatively lower (22Rv1) tracer uptake. We found that radiotracer distribution was qualitatively similar, and most abundant around the periphery of the tumor as expected for a large immunoglobulin like 4A06 (Supplemental Figure 5). Lastly, we compared ^{68}Ga-PSMA 11 uptake to ^{89}Zr-4A06 uptake in intact male mice bearing LTL-484 tumors (n = 4). Consistent with the protein expression patterns, ^{89}Zr-4A06 uptake in tumors was significantly higher than ^{68}Ga-PSMA 11 (Figure 3E).

Radioligand therapy with ^{177}Lu-4A06 inhibits mCRPC tumor growth:

We next tested if CDPC1 can be targeted for RLT in mCRPC tumors. We first tested antitumor effects in PSMA-null tumors. Intact male nu/nu mice bearing PSMA-negative DU145 tumors received ^{177}Lu-4A06 in two fractions of 400 μCi at day 0 and day 5 of the study. We chose this dosing regimen as we previously showed it to be more efficacious that a single fraction of the same total radioactive dose (i.e. 800 μCi) (14). SPECT/CT imaging showed effective tumor targeting at 72 hours after the first injection (Figure 4A). ^{177}Lu-4A06 treatment significantly delayed tumor growth compared to vehicle with no evidence for unhealthy weight loss (Figure 4B and Supplemental Figures 6–7). To test if CDCP1 RLT is efficacious against AR-positive, PSMA-positive tumors, we treated intact male nu/nu mice bearing subcutaneous C4-2B tumors with ^{177}Lu-4A06 (2 fractions of 300 μCi at day 0 and 5) or vehicle. ^{177}Lu-4A06 significantly inhibited tumor growth in this model as well, and tumor regressions were observed in two of five mice (Figure 4C–4D and Supplemental Figures 8 and 9).

Discussion

In this report, we demonstrate for the first time that CDCP1 directed RLT may be a potential therapeutic strategy for the treatment of mCRPC, including subtypes that cannot be addressed with PSMA-directed RLT or bone seeking radionuclides. This finding was enabled by expression analysis in mCRPC biopsies, which revealed that CDCP1 was expressed at the cell surface in over 60% of mCRPC biopsies, including in adenocarcinomas with negligible PSMA expression. Full length and/or cleaved CDCP1 was expressed in the majority of PSMA-null SCNC PDX models and in the majority of adenocarcinoma

PDX models, including LTL-484 which has low PSMA expression. Our study demonstrates the feasibility of detecting CDCP1 expression on prostate cancer tumors in vivo using ^{89}Zr-4A06 PET. Moreover, we showed that ^{177}Lu-4A06 significantly suppressed the growth of PSMA-null DU145 tumors and induced tumor regression in mice bearing C4-2B tumors. Collectively, these data provide the foundation to begin translational studies evaluating CDPC1-directed RLT as a treatment strategy for mCRPC.

The broad expression of CDCP1 in both adenocarcinoma and SCNC raises the question as to what signaling pathway(s) promote CDCP1 overexpression in mCRPC. The best studied regulator of CDPC1 expression, namely the RAS/Raf/Erk signaling axis (26), is not commonly hyperactive in either subtype of mCRPC. Alternatively, CDCP1 expression may be elevated transcriptionally by one of the hypoxia inducible factors, as CDCP1 was previously found to be a HIF2α target gene and HIFs can be activated downstream of mTORC1, which can be hyperactive in mCRPC (27–29). The observation that PTEN null tumors have higher CDCP1 expression would support this model. CDCP1 may also be regulated by androgen signaling in prostate cancer as LNCaP cells chronically treated with enzalutamide in charcoal stripped serum showed higher levels of CDCP1 compared to the parental cell line (9). Future mechanistic studies are required to elaborate the signaling pathways that promote and repress CDPC1 expression in prostate cancer, which may in turn lead to rational combination treatment strategies with CDCP1-directed therapeutics. Moreover, these studies may further elaborate the functional role of CDCP1 in prostate cancer, which remains elusive outside a recent observation suggesting that CDCP1 may have oncogenic properties when combined with prostate specific deletion of PTEN (9).

As CDCP1 is cleaved on the cell surface by proteases like matriptase (30), an antibody like 4A06 that recognizes an epitope on the N terminus in both full length and cleaved could be viewed as suboptimal for drug development. Indeed, one might expect that some portion of ^{89}Zr-4A06 would remain in circulation bound to a shed CDCP1 fragment. However, we do not observe unusually high levels of ^{89}Zr-4A06 compared to other radiolabeled CDCP1 antibodies. Mechanistically, we attribute this observation to our recent discovery that the cleaved N terminal CUB domain remains tightly bound to CDCP1 (16). Thus, co-targeting full length and cleaved may be a desirable approach for targeted radiotherapy.

There are several limitations of this study. As with many studies involving prostate cancer, the limited number and molecular diversity of high quality human models precludes drawing general conclusions from preclinical observations alone. Second, although we have analyzed a reasonably large RNA-seq data set, we have analyzed protein expression in a smaller cohort of patient biopsies. This is a reflection of the ongoing challenges with acquiring evaluable tissue from mCRPC biopsies, which tend to be osseous, enriched with stromal cells, and therefore challenging to isolate. Nevertheless, we are hopeful the data reported herein will inspire the community to continue to analyze mCRPC tissues for CDCP1 expression to determine its promise as a drug target while non-invasive imaging tools are brought online clinically.

Our study comes at an exciting time, as several classes of therapeutics that synergize with ionizing radiation have achieved regulatory approval for prostate cancer treatment. Examples

include the PARP inhibitor olaparib and antiandrogens like enzalutamide and apalutamide that repress DNA damage repair machinery but also may induce CDCP1 expression (9, 31, 32). The nuclear medicine community is just beginning to explore in patients the feasibility and efficacy of combination treatments with RLTs, and the early antitumor data are very encouraging.(33–36) Thus, combining CDCP1 directed RLT with standard of care treatments for mCRPC may be a potential strategy to achieve deeper clinical responses.

Supplementary Material

Refer to Web version on PubMed Central for supplementary material.

Acknowledgments

We gratefully acknowledge Dr. Henry VanBrocklin, Dr. Denis Beckford-Vera, and Joseph Blecha for assistance with radiochemistry and Ryan Tang for assistance with small animal PET/CT studies. Small animal PET/CT and SPECT/CT studies were performed on instruments supported by National Institutes of Health grants S10RR023051 and S10OD012301. We acknowledge the UCSF Helen Diller Family Comprehensive Cancer Center Tissue Core for performing immunohistochemistry.

This research was supported by a Stand Up To Cancer – Prostate Cancer Foundation – Prostate Dream Team Translational Cancer Research Grant. This research grant is made possible by the generous support of the Movember Foundation. Stand Up To Cancer is a division of the Entertainment Industry Foundation. The indicated SU2C grant is administered by the American Association for Cancer Research J.A.W. acknowledges funding from NCI 1P41CA196276, CA191018, NIH GM097316; and Bristol Meyer Squibb. J.Z. was supported by an NIH post-doctoral fellowship. J.C. was supported by a Prostate Cancer Foundation Young Investigator Award and the Department of Defense Prostate Cancer Research Program (W81XWH2010136). M. J. Evans acknowledges funding from the Congressionally Directed Medical Research Programs (W81XWH-21-1-0498) American Cancer Society (130635-RSG-17-005-01-CCE), and the Precision Imaging of Cancer and Therapy program at UCSF.

References:

1. Sgouros G, Bodei L, McDevitt MR, and Nedrow JR. Radiopharmaceutical therapy in cancer: clinical advances and challenges. Nat Rev Drug Discov. 2020;19(9):589–608. [PubMed: 32728208]
2. Jadvar H, Chen X, Cai W, and Mahmood U. Radiotheranostics in Cancer Diagnosis and Management. Radiology. 2018;286(2):388–400. [PubMed: 29356634]
3. Zoller F, Eisenhut M, Haberkorn U, and Mier W. Endoradiotherapy in cancer treatment--basic concepts and future trends. Eur J Pharmacol. 2009;625(1–3):55–62. [PubMed: 19836381]
4. Filippi L, Chiaravalloti A, Schillaci O, Cianni R, and Bagni O. Theranostic approaches in nuclear medicine: current status and future prospects. Expert Rev Med Devices. 2020;17(4):331–43. [PubMed: 32157920]
5. Sartor O, de Bono J, Chi KN, Fizazi K, Herrmann K, Rahbar K, et al. Lutetium-177-PSMA-617 for Metastatic Castration-Resistant Prostate Cancer. N Engl J Med. 2021.
6. Hofman MS, Emmett L, Sandhu S, Iravani A, Joshua AM, Goh JC, et al. [(177)Lu]Lu-PSMA-617 versus cabazitaxel in patients with metastatic castration-resistant prostate cancer (TheraP): a randomised, open-label, phase 2 trial. Lancet. 2021;397(10276):797–804. [PubMed: 33581798]
7. Leibowitz R, Davidson T, Gadot M, Aharon M, Malki A, Levartovsky M, et al. A Retrospective Analysis of the Safety and Activity of Lutetium-177-PSMA Radionuclide Treatment in Older Patients with Metastatic Castration-Resistant Prostate Cancer. Oncologist. 2020.
8. Aggarwal R, Zhang T, Small EJ, and Armstrong AJ. Neuroendocrine prostate cancer: subtypes, biology, and clinical outcomes. J Natl Compr Canc Netw. 2014;12(5):719–26. [PubMed: 24812138]
9. Alajati A, D'Ambrosio M, Troiani M, Mosole S, Pellegrini L, Chen J, et al. CDCP1 overexpression drives prostate cancer progression and can be targeted in vivo. J Clin Invest. 2020;130(5):2435–50. [PubMed: 32250342]

10. Siva AC, Wild MA, Kirkland RE, Nolan MJ, Lin B, Maruyama T, et al. Targeting CUB domain-containing protein 1 with a monoclonal antibody inhibits metastasis in a prostate cancer model. Cancer Res. 2008;68(10):3759–66. [PubMed: 18483259]
11. Yang L, Dutta SM, Troyer DA, Lin JB, Lance RA, Nyalwidhe JO, et al. Dysregulated expression of cell surface glycoprotein CDCP1 in prostate cancer. Oncotarget. 2015;6(41):43743–58. [PubMed: 26497208]
12. Kryza T, Khan T, Puttick S, Li C, Sokolowski KA, Tse BW, et al. Effective targeting of intact and proteolysed CDCP1 for imaging and treatment of pancreatic ductal adenocarcinoma. Theranostics. 2020;10(9):4116–33. [PubMed: 32226543]
13. Martinko AJ, Truillet C, Julien O, Diaz JE, Horlbeck MA, Whiteley G, et al. Targeting RAS-driven human cancer cells with antibodies to upregulated and essential cell-surface proteins. Elife. 2018;7.
14. Moroz A, Wang YH, Sharib JM, Wei J, Zhao N, Huang Y, et al. Theranostic Targeting of CUB Domain Containing Protein 1 (CDCP1) in Pancreatic Cancer. Clin Cancer Res. 2020;26(14):3608–15. [PubMed: 32341034]
15. Harrington BS, He Y, Khan T, Puttick S, Conroy PJ, Kryza T, et al. Anti-CDCP1 immuno-conjugates for detection and inhibition of ovarian cancer. Theranostics. 2020;10(5):2095–114. [PubMed: 32104500]
16. Lim SA, Zhou J, Martinko AJ, Wang YH, Filippova EV, Steri V, et al. Targeting a proteolytic neoepitope on CUB domain containing protein 1 (CDCP1) for RAS-driven cancers. J Clin Invest. 2022;132(4).
17. Hope TA, Truillet C, Ehman EC, Afshar-Oromieh A, Aggarwal R, Ryan CJ, et al. 68Ga-PSMA-11 PET Imaging of Response to Androgen Receptor Inhibition: First Human Experience. J Nucl Med. 2017;58(1):81–4. [PubMed: 27660139]
18. Quigley DA, Dang HX, Zhao SG, Lloyd P, Aggarwal R, Alumkal JJ, et al. Genomic Hallmarks and Structural Variation in Metastatic Prostate Cancer. Cell. 2018;175(3):889. [PubMed: 30340047]
19. Aggarwal RR, Quigley DA, Huang J, Zhang L, Beer TM, Rettig MB, et al. Whole-Genome and Transcriptional Analysis of Treatment-Emergent Small-Cell Neuroendocrine Prostate Cancer Demonstrates Intraclass Heterogeneity. Mol Cancer Res. 2019;17(6):1235–40. [PubMed: 30918106]
20. Altman DG, and Bland JM. Statistics notes. Treatment allocation in controlled trials: why randomise? BMJ. 1999;318(7192):1209. [PubMed: 10221955]
21. Casar B, Rimann I, Kato H, Shattil SJ, Quigley JP, and Deryugina EI. In vivo cleaved CDCP1 promotes early tumor dissemination via complexing with activated beta1 integrin and induction of FAK/PI3K/Akt motility signaling. Oncogene. 2014;33(2):255–68. [PubMed: 23208492]
22. Wright HJ, Arulmoli J, Motazedi M, Nelson LJ, Heinemann FS, Flanagan LA, et al. CDCP1 cleavage is necessary for homodimerization-induced migration of triple-negative breast cancer. Oncogene. 2016;35(36):4762–72. [PubMed: 26876198]
23. Casar B, He Y, Iconomou M, Hooper JD, Quigley JP, and Deryugina EI. Blocking of CDCP1 cleavage in vivo prevents Akt-dependent survival and inhibits metastatic colonization through PARP1-mediated apoptosis of cancer cells. Oncogene. 2012;31(35):3924–38. [PubMed: 22179830]
24. Wang X, Ma D, Olson WC, and Heston WD. In vitro and in vivo responses of advanced prostate tumors to PSMA ADC, an auristatin-conjugated antibody to prostate-specific membrane antigen. Mol Cancer Ther. 2011;10(9):1728–39. [PubMed: 21750220]
25. Sharma SK, Chow A, Monette S, Vivier D, Pourat J, Edwards KJ, et al. Fc-Mediated Anomalous Biodistribution of Therapeutic Antibodies in Immunodeficient Mouse Models. Cancer Res. 2018;78(7):1820–32. [PubMed: 29363548]
26. Uekita T, Fujii S, Miyazawa Y, Iwakawa R, Narisawa-Saito M, Nakashima K, et al. Oncogenic Ras/ERK signaling activates CDCP1 to promote tumor invasion and metastasis. Mol Cancer Res. 2014;12(10):1449–59. [PubMed: 24939643]
27. Emerling BM, Benes CH, Poulogiannis G, Bell EL, Courtney K, Liu H, et al. Identification of CDCP1 as a hypoxia-inducible factor 2alpha (HIF-2alpha) target gene that is associated with

survival in clear cell renal cell carcinoma patients. Proc Natl Acad Sci U S A. 2013;110(9):3483–8. [PubMed: 23378636]

28. Zhong H, Chiles K, Feldser D, Laughner E, Hanrahan C, Georgescu MM, et al. Modulation of hypoxia-inducible factor 1alpha expression by the epidermal growth factor/phosphatidylinositol 3-kinase/PTEN/AKT/FRAP pathway in human prostate cancer cells: implications for tumor angiogenesis and therapeutics. Cancer Res. 2000;60(6):1541–5. [PubMed: 10749120]
29. Majumder PK, Febbo PG, Bikoff R, Berger R, Xue Q, McMahon LM, et al. mTOR inhibition reverses Akt-dependent prostate intraepithelial neoplasia through regulation of apoptotic and HIF-1-dependent pathways. Nat Med. 2004;10(6):594–601. [PubMed: 15156201]
30. He Y, Wortmann A, Burke LJ, Reid JC, Adams MN, Abdul-Jabbar I, et al. Proteolysis-induced N-terminal ectodomain shedding of the integral membrane glycoprotein CUB domain-containing protein 1 (CDCP1) is accompanied by tyrosine phosphorylation of its C-terminal domain and recruitment of Src and PKCdelta. J Biol Chem. 2010;285(34):26162–73. [PubMed: 20551327]
31. Polkinghorn WR, Parker JS, Lee MX, Kass EM, Spratt DE, Iaquinta PJ, et al. Androgen receptor signaling regulates DNA repair in prostate cancers. Cancer Discov. 2013;3(11):1245–53. [PubMed: 24027196]
32. Spratt DE, Evans MJ, Davis BJ, Doran MG, Lee MX, Shah N, et al. Androgen Receptor Upregulation Mediates Radioresistance after Ionizing Radiation. Cancer Res. 2015;75(22):4688–96. [PubMed: 26432404]
33. Purohit NK, Shah RG, Adant S, Hoepfner M, Shah GM, and Beauregard JM. Potentiation of (177)Lu-octreotate peptide receptor radionuclide therapy of human neuroendocrine tumor cells by PARP inhibitor. Oncotarget. 2018;9(37):24693–706. [PubMed: 29872498]
34. Nonnekens J, van Kranenburg M, Beerens CE, Suker M, Doukas M, van Eijck CH, et al. Potentiation of Peptide Receptor Radionuclide Therapy by the PARP Inhibitor Olaparib. Theranostics. 2016;6(11):1821–32. [PubMed: 27570553]
35. Chen H, Zhao L, Fu K, Lin Q, Wen X, Jacobson O, et al. Integrin alphavbeta3-targeted radionuclide therapy combined with immune checkpoint blockade immunotherapy synergistically enhances anti-tumor efficacy. Theranostics. 2019;9(25):7948–60. [PubMed: 31695808]
36. Choi J, Beaino W, Fecek RJ, Fabian KPL, Laymon CM, Kurland BF, et al. Combined VLA-4-Targeted Radionuclide Therapy and Immunotherapy in a Mouse Model of Melanoma. J Nucl Med. 2018;59(12):1843–9. [PubMed: 29959213]

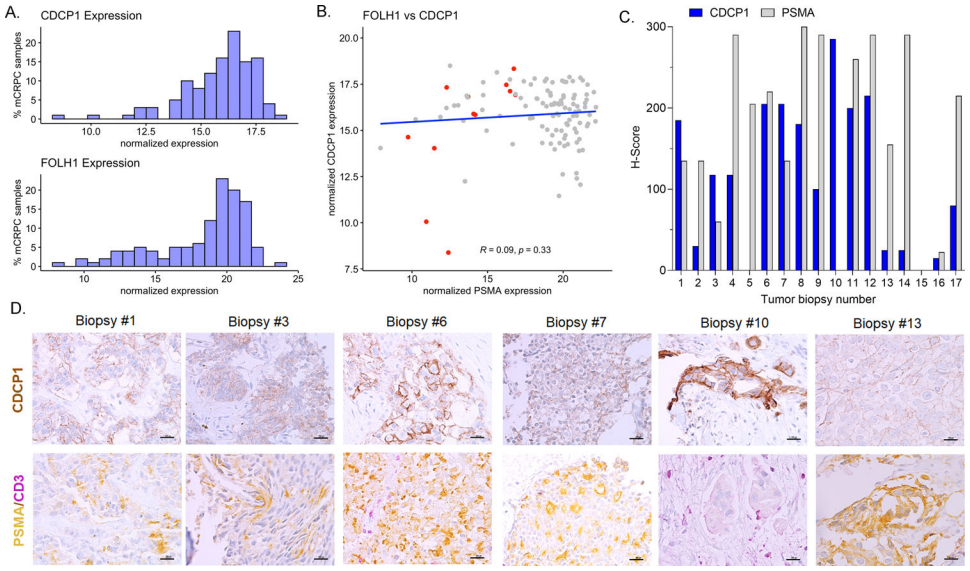

Figure 1. CDCP1 is expressed in mCRPC.

A. Histograms showing the distribution of *CDCP1* mRNA levels over the set of 119 mCRPC biopsies. *FOLH1* (PSMA), an abundantly expressed target for radioligand therapy, is shown for comparison. **B**. A scatter plot showing the expression of *CDPC1* and *FOLH1* per biopsy. A Pearson correlation shows no significant trend in expression between the two genes. SCNC tumors are highlighted in red. **C**. A graphical summary of the mean H-scores for CDCP1 membrane staining from 17 evaluable mCRPC biopsies. The H-scores were determined by two blinded pathologists and the mean reported. Four of seventeen biopsies (23%) had higher CDCP1 H-scores compared to PSMA. All biopsies were histologically adenocarcinoma. **D**. Representative IHC images for CDCP1 (brown) and PSMA/CD3 (gold and magenta) in PSMA-high and PSMA-low metastatic prostate cancer biopsies. The scale bar indicates a length of 100 μm.

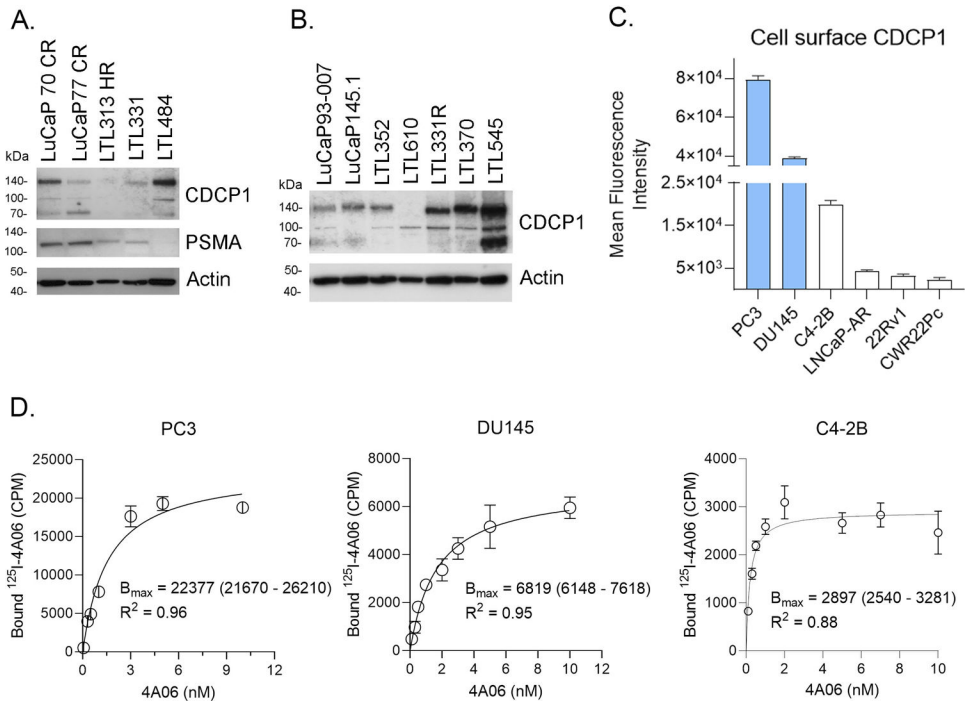

Figure 2. CDCP1 is abundantly expressed in human prostate cancer models, including PSMA low adenocarcinoma and SCNC.

A. Immunoblot data showing CDCP1 expression in human prostate cancer adenocarcinoma PDX whole cell lysates. **B**. Immunoblot data showing CDCP1 expression in human SCNC prostate cancer PDX whole cell lysates. **C**. Flow cytometry data showing the relative levels of total (full length and cleaved) cell surface CDCP1 in six human prostate cancer cell lines. AR and PSMA negative cell lines are shaded in blue. **D**. Saturation binding assays with ^{125}I-4A06 performed on PC3, DU145, and C4-2B cells. The B_{max} (95% confidence intervals) values and R^2 values are reported inset for each study.

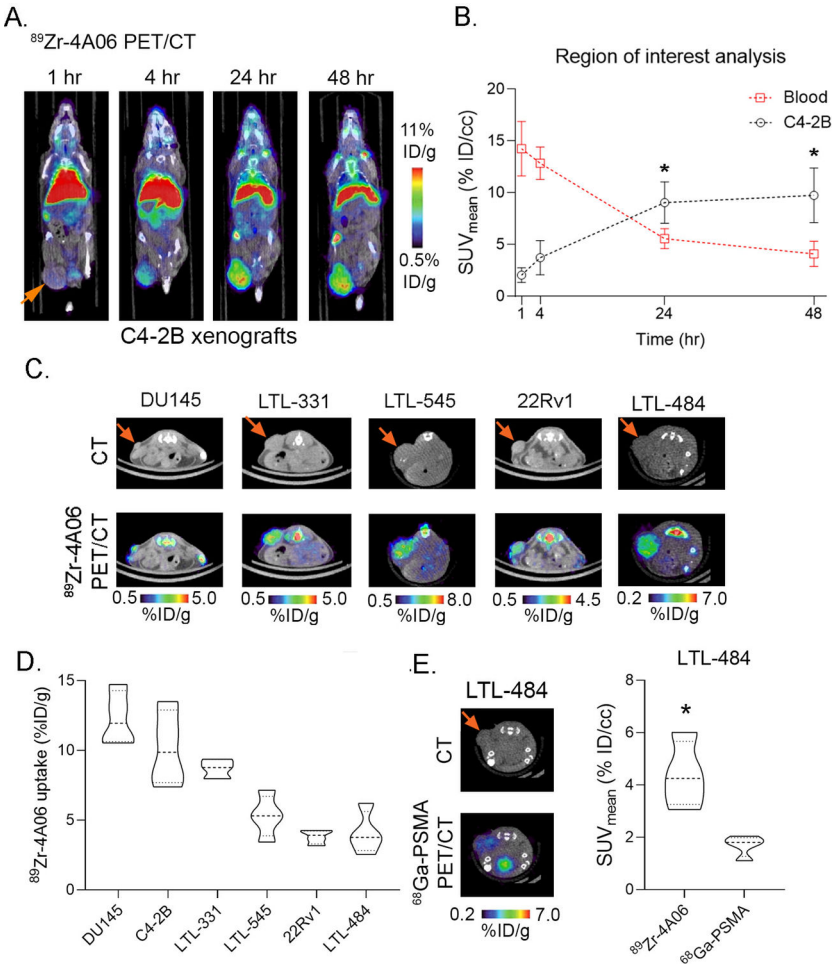

Figure 3. CDCP1 expression is measurable in vivo with ^{89}Zr-4A06 PET on prostate cancer tumors, including those with low or negligible PSMA expression.

A. Representative coronal PET/CT images showing the biodistribution of ^{89}Zr-4A06 over time in intact male nu/nu mice bearing subcutaneous C4-2B tumors. The position of the tumor is indicated with an orange arrow. **B**. A line graph showing the radiotracer uptake in tumor and blood pool over time. The data were acquired using region of interest analysis of the PET data from a cohort of four mice imaged serially with PET/CT. *P<0.01. **C**. Transaxial CT and PET/CT images showing the tumoral uptake of ^{89}Zr-4A06 at 48 hours post injection in two PSMA low adenocarcinoma and two SCNC tumor types. The arrows indicate the position of the subcutaneous tumor. **D**. Biodistribution data showing the tumoral uptake of ^{89}Zr-4A06 at 48 hours post injection. The data were acquired from cohort sizes of n = 4/tumor. **E**. Transaxial ^{68}Ga-PSMA 11 PET/CT data in a mouse bearing PSMA low LTL-484 tumors. The position of the tumor is indicated with an orange arrow, and the imaged is scaled to match the ^{89}Zr-4A06 data in panel C for comparison. The image was acquired at 45 minutes post injection. At right is depicted SUVmean data acquired from mice bearing LTL-484 tumors (n = 4). Each mouse was imaged first with ^{68}Ga-PSMA 11, and then after 6 days, ^{89}Zr-4A06. The images were acquired 45 minutes post injection of ^{68}Ga-PSMA 11, and 48 hours after injection of ^{89}Zr-4A06. *P<0.01

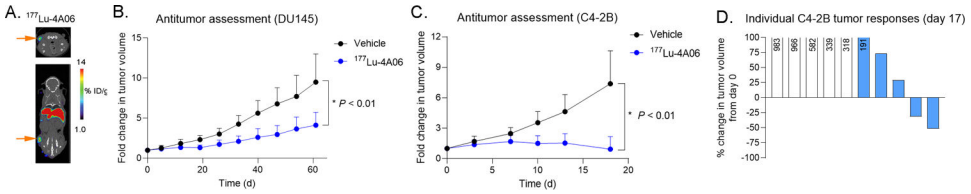

Figure 4. ^{177}Lu-4A06 monotherapy inhibits the growth of prostate cancer tumors.

A. A SPECT/CT image showing tumoral localization of ^{177}Lu-4A06 in a mouse bearing a subcutaneous DU145 tumor (orange arrow). The image was acquired at 48 hours after a second injection of 400 μCi of ^{177}Lu-4A06 (i.e. 8 days after the start of the study). **B**. An antitumor assessment study showing the suppression of DU145 tumor growth by ^{177}Lu-4A06, administered in two fractions on day 0 and day 5, 400 μCi/dose. The volume of each tumor was normalized to the initial volume at day 0 of the study. The difference in tumor growth between treatment arms was significant, P<0.01. **C** An antitumor assessment study showing the suppression of C4-2B tumor growth by ^{177}Lu-4A06, administered in two fractions on day 0 and day 5, 300 μCi/dose. The volume of each tumor was normalized to the initial volume at day 0 of the study. The difference in tumor growth between treatment arms was significant, P<0.01. **D**. A waterfall plot showing percent change in tumor volume for individual tumors from the C4-2B cohort. Bars shaded white represent tumors from mice receiving vehicle, and bars shaded light blue represent tumors from mice that received ^{177}Lu-4A06. For those bars that extend off the scale, the percent change in tumor volume is listed within the respective bar.

Table 1.

Differential gene expression analysis of PTEN and CDCP1 between patients with any type of PTEN mutation (deletion, inversion, break-end) versus wild type PTEN.

Gene	Log2 Fold Change	Unadjusted P value	False discovery rate
PTEN	−1.44	2.1×10^{-6}	0.04
CDCP1	0.52	0.20	0.88